Journal of Materials Chemistry A

ROYAL SOCIETY OF CHEMISTRY

PAPER

View Article Online
View Journal | View Issue

Cite this: *J. Mater. Chem. A*, 2021, **9**, 9165

The effect of the position of cross-linkers on the structure and microenvironment of PPh_3 moiety in porous organic polymers†

Guangjun Ji,‡[ab] Cunyao Li,‡[a] Dong Xiao,[c] Guoqing Wang,[ab] Zhao Sun,[ab] Miao Jiang,[a] Guangjin Hou, *[c] Li Yan*[a] and Yunjie Ding *[ac]

Received 20th December 2020
Accepted 11th March 2021

DOI: 10.1039/d0ta12316a

rsc.li/materials-a

Three trivinyl functionalization triphenylphosphine ($3vPPh_3$)-based porous organic ligands ($3vPPh_3$-POLs) with cross-linkers in different positions were obtained through solvothermal polymerization. By simply changing the position of the cross-linkers (vinyl groups) attached to the PPh_3 monomer, the resulting porous organic polymer (POP) materials acquired diverse hierarchical porous structures, and the microenvironment of POPs was sequently regulated. Among the three $3vPPh_3$-POLs, the BET surface areas ranged from 168 to 1583 $m^2\ g^{-1}$, while the proportion of micropores changed from 0.0% to 52.0%. Benefiting from the unique structure, Rh ions could be coordinated and dispersed as a single site in *m*-$3vPPh_3$-POL to form $HRh(CO)_2(PPh_3\text{-POL})_2$ species, which endowed the Rh/*m*-$3vPPh_3$-POL catalyst with an activity similar to that in the homogeneous system, an *l*/*b* ratio (the ratio of the linear aldehyde to the branched aldehyde) approximately as high as 10, and stability for a duration of more than 500 h in the hydroformylation of 1-octene.

1 Introduction

As a new class of functional materials, porous organic polymers (POPs) have got the full attention of researchers due to their extensive application in gas sorption and storage,[1] energy storage,[2] proton conduction[3] and catalysis.[4–7] The POP family consists of hyper-cross-linked polymers (HCPs),[8] polymers of intrinsic microporosity (PIMs),[9] conjugated microporous polymers (CMPs)[10] and covalent organic frameworks (COFs).[11] Various cross-linking methods have been employed to fabricate these elegant materials, for example, COFs can be cross-linked by boroxine,[12] boronate ester,[13] imine,[14] triazine,[15] *etc.* HCPs can be fabricated by external crosslinking,[16] post-crosslinking[17] or direct polycondensation.[18] PIMs are prepared by the formation of dibenzodioxin[19] and formation of imide linkages.[20] CMPs are prepared by the polymerization of monomers with conjugate structures.[21]

A series of CMPs was prepared through the Sonogashira cross-linking reaction of 1,3,5-triethynyl-benzene (C≡C) with bipyridine in our previous study. The characterization result illustrated that the C≡C groups could cooperate with N atoms from pyridine to coordinate with Pd(II), and served as both cross-linkers and coordination sites. The pyridine-based CMP could be used as a heterogeneous ligand for the Pd(II)-catalyzed oxidative Heck reaction with high linear selectivity (the ratio of linear products to branched products was more than 100 : 1).[22] We also introduced vinyl groups to organic ligand monomers and prepared a new kind of POPs through solvothermal polymerization, denoted as porous organic ligands (POLs). POLs possess high surface area, large pore volume, hierarchical porosity, favorable stability, and highly exposed functional sites.[23] Compared with other fabricating methods, the polymerization of vinyl groups in functional monomers is believed to be the most effective and relatively cheaper way to get functional POPs. Recently, a series of POLs has been constructed and used in many fields.[24–28] It is worth mentioning that we have achieved the industrial production and application of POLs as a bifunctional material to prepare a heterogeneous catalyst for the hydroformylation of ethylene. However, the effects of the position of cross-linkers and the intrinsic structure of monomers on the properties of POLs are very far from being understood.

Based on our previous works, we believe that the properties of POPs could be optimized by regulating the skeletons; herein, we provide a new strategy to regulate the skeletons of POPs by simply changing the position of the vinyl groups attached to the functional monomer. Tris(vinphenyl)phosphine ($3vPPh_3$) was employed as a template to demonstrate the feasibility of this regulation strategy. Three $3vPPh_3$-POLs were prepared according to this strategy, and each of them displayed different

[a]*Dalian National Laboratory for Clean Energy, Dalian Institute of Chemical Physics, Chinese Academy of Sciences, Dalian, 116023, P. R. China. E-mail: yanli@dicp.ac.cn; dyj@dicp.ac.cn*

[b]*University of Chinese Academy of Sciences, Beijing 100039, P. R. China*

[c]*State Key Laboratory of Catalysis, Dalian Institute of Chemical Physics, Chinese Academy of Sciences, Dalian, 116023, P. R. China. E-mail: ghou@dicp.ac.cn*

† Electronic supplementary information (ESI) available. See DOI: 10.1039/d0ta12316a

‡ These authors contributed equally to this work.

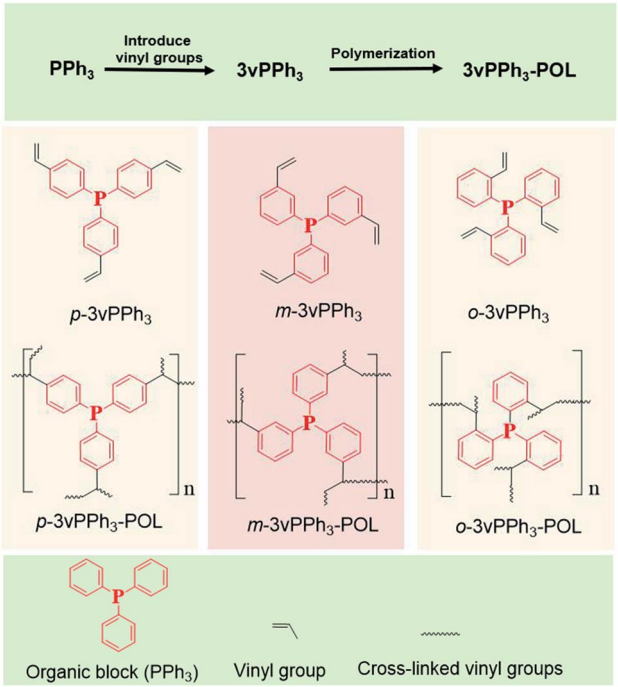

Scheme 1 The preparation method of the three $3vPPh_3$ monomers and their corresponding POLs; the three $3vPPh_3$ monomers were constituted by the same organic block and vinyl group, while possessing different structures.

structures. Also, Rh ions were introduced into these $3vPPh_3$-POLs (denoted as Rh/$3vPPh_3$-POLs) to further validate the transformation of the microenvironment of the PPh_3 moiety among these $3vPPh_3$-POLs, as Rh–P complexes are sensitive in hydroformylation reaction. Scheme 1 shows the regulation strategy and structures of the three $3vPPh_3$ monomers and the corresponding $3vPPh_3$-POLs. The characterization of Rh/$3vPPh_3$-POLs by MAS NMR, EXAFS and *in situ* FTIR illustrated that the microenvironment of the PPh_3 moiety was different when the three $3vPPh_3$-POLs were coordinated with Rh ions.

2 Experimental

2.1 Materials

All solvents were purified according to standard laboratory methods. Azobisisobutyronitrile (AIBN) (99%), tetrahydrofuran (THF) (99%) and PCl_3 (97%) were purchased from Tianjin Kemiou Chemical Reagent Co., Ltd. $Rh(CO)_2(acac)$ (99%), 1-hexene (97%), 1-octene (99%), 1-heptene (98%) and 1-dodecene (97%) were obtained from J&K Scientific Ltd. Sodium (98%), benzophenone (98%), 4-bromostyrene (98%), 3-bromostyrene (98%) and 2-bromostyrene (98%) were obtained from Aladdin. THF was distilled over sodium/benzophenone under Ar atmosphere, and PCl_3 was purified by distillation under Ar atmosphere before use.

2.2 Methods

Unless otherwise noted, all manipulations were carried out under Ar atmosphere in a glove-box or using standard Schlenk techniques.

Synthesis of *p*-$3vPPh_3$, *m*-$3vPPh_3$ and *o*-$3vPPh_3$

Synthesis of p-3vPPh₃. First, 60 mmol 4-bromostyrene was dissolved in 60 mL THF, added dropwise to 63 mmol magnesium chips in 1 hour, then reacted for 4 hours to get solution A. Next, 20 mmol PCl_3 was dissolved in 20 mL THF, added dropwise to solution A at 253 K in 1 hour, then reacted for 2 hours. After the reaction, 50 mL of saturated NH_4Cl aqueous was added. The organic phase was extracted with excessive amount of ethyl acetate, which was dried with $MgSO_4$. After filtering and purifying by silica gel chromatography (EtOAc/Petroleum ether = 1/20), *p*-$3vPPh_3$ (white solid) was obtained. ^{1}H NMR (400 MHz, chloroform-d) δ 7.41–7.32 (m, 6H), 7.27 (t, J = 7.8 Hz, 6H), 6.70 (dd, J = 17.6, 10.9 Hz, 3H), 5.77 (d, J = 17.6 Hz, 3H), 5.27 (d, J = 10.9 Hz, 3H). ^{13}C NMR (101 MHz, chloroform-d) δ 138.03, 136.62 (d, J = 10.6 Hz), 136.39, 133.91 (d, J = 19.6 Hz), 126.35 (d, J = 7.1 Hz), 114.74. ^{31}P NMR (162 MHz, chloroform-d) δ −6.76.

Synthesis of m-3vPPh₃. Under the same conditions as *p*-$3vPPh_3$. On replacing 4-bromostyrene with 3-bromostyrene, *m*-$3vPPh_3$ (pale yellow oil) was obtained. ^{1}H NMR (400 MHz, chloroform-d) δ 7.46–7.34 (m, 6H), 7.28 (td, J = 8.3, 7.9, 1.4 Hz, 3H), 7.18 (d, J = 7.2 Hz, 3H), 6.63 (dd, J = 17.6, 10.9 Hz, 3H), 5.66 (d, J = 18.2 Hz, 3H), 5.20 (d, J = 11.5 Hz, 3H). ^{13}C NMR (101 MHz, chloroform-d) δ 137.76 (d, J = 7.7 Hz), 137.29 (d, J = 11.2 Hz), 136.54, 133.07 (d, J = 16.5 Hz), 131.96 (d, J = 23.0 Hz), 128.80 (d, J = 6.3 Hz), 126.58, 114.50. ^{31}P NMR (162 MHz, chloroform-d) δ −5.10.

Synthesis of o-3vPPh₃. Under the same conditions as *p*-$3vPPh_3$. On replacing 4-bromostyrene with 2-bromostyrene, *o*-$3vPPh_3$ (white solid) was obtained. ^{1}H NMR (400 MHz, chloroform-d) δ 7.59 (dd, J = 7.3, 4.5 Hz, 3H), 7.46–7.20 (m, 6H), 7.12 (t, J = 7.4 Hz, 3H), 6.74 (dd, J = 7.6, 4.4 Hz, 3H), 5.61 (d, J = 17.2 Hz, 3H), 5.18 (d, J = 10.9 Hz, 3H). ^{13}C NMR (101 MHz, chloroform-d) δ 142.41 (d, J = 23.0 Hz), 135.41 (d, J = 24.6 Hz), 134.07, 133.69 (d, J = 12.3 Hz), 129.04, 127.93, 125.47 (d, J = 4.5 Hz), 115.83. ^{31}P NMR (162 MHz, chloroform-d) δ −29.65.

Synthesis of *p*-$3vPPh_3$-POL, *m*-$3vPPh_3$-POL and *o*-$3vPPh_3$-POL

Synthesis of p-3vPPh₃-POL. First, 1.0 g *p*-$3vPPh_3$ and 25.0 mg AIBN were dissolved in 10 mL THF. After stirring for 30 minutes at room temperature, the mixture was transferred into an autoclave, then maintained at 373 K for 24 h. After evaporation of THF under vacuum, the polymer *p*-$3vPPh_3$-POL was obtained as a white solid.

Synthesis of m-3vPPh₃-POL. First, 1.0 g *m*-$3vPPh_3$ and 25.0 mg AIBN were dissolved in 10 mL THF. After stirring for 30 minutes at room temperature, the mixture was transferred into an autoclave, then maintained at 373 K for 24 h. After evaporation of THF under vacuum, the polymer *m*-$3vPPh_3$-POL was obtained as a white solid.

Synthesis of o-3vPPh₃-POL. First, 1.0 g *o*-$3vPPh_3$ and 25.0 mg AIBN were dissolved in 10 mL THF. After string for 30 minutes at room temperature, the mixture was transferred into an autoclave, then maintained at 373 K for 24 h. After evaporation of THF under vacuum, the polymer *o*-$3vPPh_3$-POL was obtained as a pale-yellow solid.

Synthesis of Rh/*p*-3vPPh$_3$-POL, Rh/*m*-3vPPh$_3$-POL and Rh/*o*-3vPPh$_3$-POL

Synthesis of Rh/p-3vPPh$_3$-POL. One gram *p*-3vPPh$_3$-POL and 6.3 mg Rh(acac)(CO)$_2$ were added to 30 mL THF. After stirring for 24 h at room temperature, the resulted product was separated by using a centrifuge. The crude product was washed with THF (3 × 5 mL). After evaporation of THF under vacuum, the slight yellow catalyst Rh/*p*-3vPPh$_3$-POL was obtained.

Synthesis of Rh/m-3vPPh$_3$-POL. One gram *m*-3vPPh$_3$-POL and 6.3 mg Rh(acac)(CO)$_2$ were added to 30 mL THF. After stirring for 24 h at room temperature, the resulted product was separated by using a centrifuge. The crude product was washed with THF (3 × 5 mL). After evaporation of THF under vacuum, the slight yellow catalyst Rh/*m*-3vPPh$_3$-POL was obtained.

Synthesis of Rh/o-3vPPh$_3$-POL. One gram *o*-3vPPh$_3$-POL and 6.3 mg Rh(acac)(CO)$_2$ were added to 30 mL THF. After stirring for 24 h at room temperature, the resulting product was separated by using a centrifuge. The crude product was washed with THF (3 × 5 mL). After evaporation of THF under vacuum, the slight yellow catalyst Rh/*o*-3vPPh$_3$-POL was obtained.

2.3 Catalytic performance tests

As a typical run for autoclave reaction, 5.0 g of toluene, 1.0 g of 1-octene, and 0.060 g of Rh/*m*-3vPPh$_3$-POL catalyst were added into an autoclave. After sealing and purging with syngas (CO : H$_2$ = 1 : 1) 6 times, the autoclave was heated to 383 K within 30 min, followed by adjusting the pressure of syngas to 1.0 MPa and stirring at 383 K for 12 h. During the reaction, the pressure in the reactor was held by the injection of syngas (CO : H$_2$ = 1 : 1) *via* a pressure regulator. After cooling the autoclave in an ice bath and releasing the pressure, a sample was taken from the autoclave by filtration or centrifugation and analyzed.

In the recycling experiment, the cooled autoclave was opened in a glove box; a filter was used to separate the catalyst, and the catalyst could be directly used in the next run.

We also performed the fixed-bed hydroformylation of long-chain olefins to test the stability of Rh/*m*-3vPPh$_3$-POL catalysts. The length of the fixed-bed reactor was 40 cm, and the inner diameter was 9 mm. As a typical run, 12 mL of quartz sand was filled at the bottom of the reactor, followed by filling in a little silica wool (<1 mL) and 0.30 g of Rh/*m*-3vPPh$_3$-POL catalyst (about 2.0 mL), then a little silica wool (<1 mL) and another 12 mL of quartz sand was filled at the top of the reactor. Thus, the catalyst was put just in the middle of the reactor. The reactor was heated by a tubular furnace and the temperature was monitored by a thermocouple which was just put in the thermocouple hole beside the sample hole. The effluent passed through a condenser to capture the liquid products. A simple flowchart of the hydroformylation equipment is listed in Scheme S1.†

The products were analyzed off-line by an Agilent 7890B gas chromatograph with an HP-5 column (30 m length, 0.3 2 mm diameter). The column temperature was initially kept at 313 K for 5 min and then raised to 373 K at 5 K min^{-1}, maintained at 373 K for 2 min then raised to 448 K at 10 K min^{-1}. Argon was used as the carrier gas and the column front pressure was kept at 4 psi. The injection port was held at 523 K, 4 psi while the split ratio was kept at 50 : 1. As for the flame ionization detector (FID), the temperature was held at 493 K and the flow rate of H$_2$ was kept at 30 mL min^{-1} while the flow rate of air was held at 300 mL min^{-1}. *n*-Butanol was used as an internal standard and the GC was also calibrated using quantitative analysis of substrates and products.

3 Results and discussion

3.1 Effects of the position of cross-linkers on the structure evolution

Firstly, as shown in the upper line of Scheme 1, three kinds of tris(vinphenyl)phosphine (3vPPh$_3$) with cross-linkers (vinyl groups) in different positions were designed and successfully synthesized by precisely controlling the position of the cross-linkers in functional monomers, and their NMR spectra are displayed in Fig. S1.† Then, the three 3vPPh$_3$-POLs were prepared through solvothermal polymerization with yields of 100%. To figure out the differences in the structure among the 3vPPh$_3$-POLs, nitrogen sorption isotherms, thermogravimetric analysis (TGA) and scanning electron microscopy (SEM) were employed to characterize the 3vPPh$_3$-POLs. Table 1 shows that *p*-3vPPh$_3$-POL, *m*-3vPPh$_3$-POL and *o*-3vPPh$_3$-POL possess different BET surface areas, from 1583 m^2 g^{-1} to 168 m^2 g^{-1}, and pore volumes, from 2.70 cm^3 g^{-1} to 0.15 cm^3 g^{-1}. As shown in Fig. 1a, both *m*-3vPPh$_3$-POL and *p*-3vPPh$_3$-POL exhibit the curve of type I plus type-IV, while *o*-3vPPh$_3$-POL does not, indicating that *m*-3vPPh$_3$-POL and *p*-3vPPh$_3$-POL possess intrinsic hierarchical porosity, which is further confirmed by the SEM images (Fig. 1d).

As calculated by non-local density functional theory (NLDFT), the pore sizes of *m*-3vPPh$_3$-POL and *p*-3vPPh$_3$-POL are distributed from 0.59 nm to 2.84 nm (Fig. 1b), while the proportion of micropores in *m*-3vPPh$_3$-POL is more than double that in *p*-3vPPh$_3$-POL (Table 1). Compared with *m*-3vPPh$_3$-POL and *p*-3vPPh$_3$-POL, *o*-3vPPh$_3$-POL possesses lower surface area and pore volume, and is mesoporous only. The TGA curves of all three 3vPPh$_3$-POLs also show different decomposition temperatures. The decomposition temperatures of *p*-3vPPh$_3$-POL and *m*-3vPPh$_3$-POL are higher than 700 K while that of *o*-3vPPh$_3$-POL is 650 K (Fig. 1c), which indicates that *p*-3vPPh$_3$-POL and *m*-3vPPh$_3$-POL possess better thermal stability. As shown in Fig. 1d–f, the SEM images exhibit the amorphous morphology of 3vPPh$_3$-POLs. Moreover, the SEM images of *p*-3vPPh$_3$-POL

Table 1 Textural parameters of *p*-3vPPh$_3$-POL, *m*-3vPPh$_3$-POL and *o*-3vPPh$_3$-POL

Samples	BET surface area (m^2 g^{-1})	Pore volume (cm^3 g^{-1})	Micropore (%)
p-3vPPh$_3$-POL	1583	2.70	23.5
m-3vPPh$_3$-POL	841	1.68	52.0
o-3vPPh$_3$-POL	168	0.15	0.0

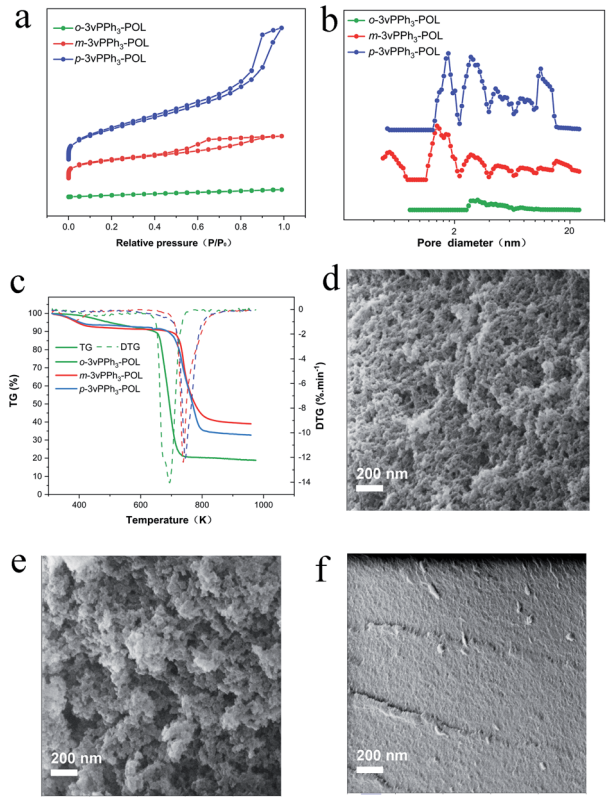

Fig. 1 (a) Nitrogen sorption isotherms of different 3vPPh$_3$-POLs materials. (b) Pore size distribution of different 3vPPh$_3$-POL materials. (c) TGA and DTG curves of different 3vPPh$_3$-POLs materials. (d) The SEM image of *p*-3vPPh$_3$-POL. (e) The SEM image of *m*-3vPPh$_3$-POL. (f) The SEM image of *o*-3vPPh$_3$-POL.

and *m*-3vPPh$_3$-POL reveal a highly developed pore structure, while that of *o*-3vPPh$_3$-POL shows a poor pore structure.

To further confirm the transformation of the framework in 3vPPh$_3$-POLs, *m*-3vPPh$_3$-POL and *p*-3vPPh$_3$-POL were characterized by the ^{13}C cross-polarization (CP) and one pulse magic angle spinning (MAS) NMR, shown in Fig. 2. The strong signals

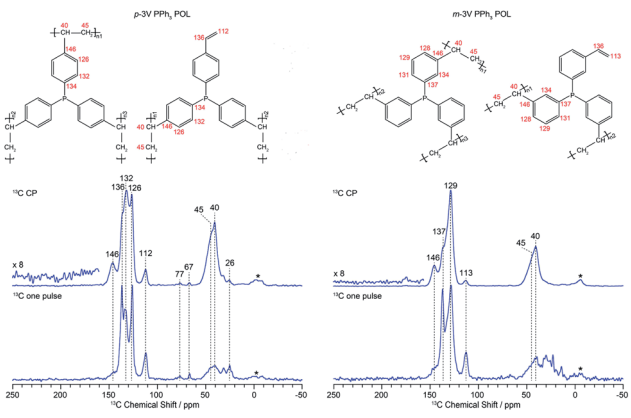

Fig. 2 ^{13}C MAS NMR spectrum of *m*-3vPPh$_3$-POL and *p*-3vPPh$_3$-POL. CP mode was employed for testing the framework structure of samples, one pulse mode provided more refined analysis of the framework structure.

ranging from 129 to 146 ppm are assigned to the aromatic carbons of 3vPPh$_3$-POLs, and the signal at 40 ppm is attributed to the polymerized vinyl groups. There is a very small peak at 112 ppm in the ^{13}C MAS NMR spectrum of *p*-3vPPh$_3$-POL, which could be assigned to unpolymerized vinyl groups, indicating that *p*-3vPPh$_3$-POL is highly polymerized.[33] Similarly, the small peak at 113 ppm in the ^{13}C MAS NMR spectra of *m*-3vPPh$_3$-POL declares its high degree of polymerization. However, the great differences in the ^{13}C CP and one pulse MAS NMR between *m*-3vPPh$_3$-POL and *p*-3vPPh$_3$-POL declare the discrepancy in their structures, which comes from the monomer gap, to be precise, the difference in the position of the vinyl groups.

To clearly clarify whether the frameworks of *p*-3vPPh$_3$-POL and *m*-3vPPh$_3$-POL are changed under external environment, the kinetic performances of the polymer frameworks were characterized by ^{13}C{^{1}H} R-type RF irradiation and two-dimensional separated local field (2D R-SLF) experiments. These experiments measure the residual ^{13}C–^{1}H dipolar coupling which is then used as an indicator to monitor the motions of the 3vPPh$_3$-POL frameworks upon post treatments and reactions. The ^{13}C–^{1}H dipolar coupling of CH groups from both aromatic rings and polymerized vinyl groups of *m*-3vPPh$_3$-POL and *p*-3vPPh$_3$-POL was measured (as shown in Fig. 3). The results show that CH groups in both *m*-3vPPh$_3$-POL and *p*-3vPPh$_3$-POL have a ^{13}C–^{1}H dipolar coupling strength of 22 kHz, indicating that the frameworks of these materials are rather rigid, since ^{13}C–^{1}H dipolar coupling for CH and CH$_2$ groups in

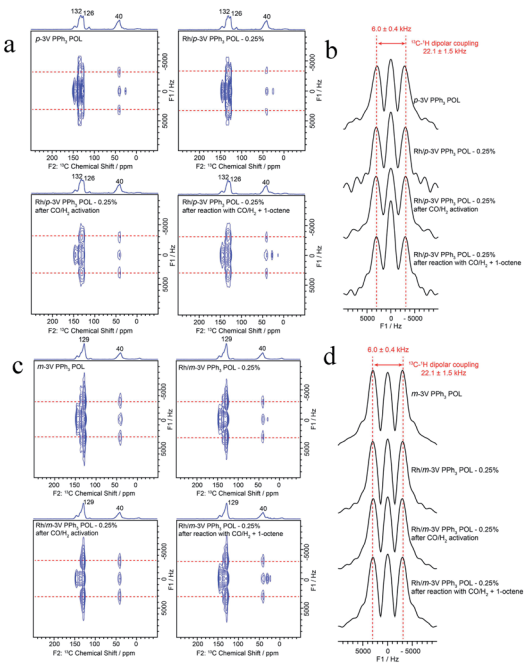

Fig. 3 (a) ^{13}C{^{1}H} 2D R-SLF spectra of *p*-3vPPh$_3$-POL and Rh/*p*-3vPPh$_3$-POL in different stages. (b) The F_1 dimension slices of ^{13}C peak at 132 ppm spectra of (a). (c) ^{13}C{^{1}H} 2D R-SLF spectra of *m*-3vPPh$_3$-POL and Rh/*m*-3vPPh$_3$-POL in different stages. (d) The F_1 dimension slices of ^{13}C peak at 132 ppm spectra of (c). The residual dipole coupling is calculated from the splitting based on the scaling factor of the recoupling sequence used.

a rigid framework retains a strength of a one-bond distance and is about 22 kHz, but less than 22 kHz when the dipolar coupling is averaged by molecular motions.[32] Also, the ^{13}C–^{1}H dipolar coupling strength of the CH groups of these POLs is retained well after Rh doping, catalyst activation and reaction, suggesting their strong structural stability upon post treatment and reaction.

3.2 Effects of the position of cross-linkers on microenvironment of 3vPPh$_3$ moiety

In 3vPPh$_3$-POLs, the functional sites are mainly presented by P in the PPh$_3$ moiety. As an embodiment of the functional sites of 3vPPh$_3$-POLs, P atoms clearly reflect the transformation of the microenvironment of the PPh$_3$ moiety in 3vPPh$_3$-POLs, by their capacity of coordinating with Rh ions.[23,31] Therefore, Rh ions were introduced to coordinate with P atoms, which could intuitively reveal the changes in the PPh$_3$ moiety.

As confirmed by our previous works, the high surface area and large pore volume of the POLs are in favor of exposing more functional P sites, which promote the dispersion and anchoring of metals.[29,30] Rh/*m*-3vPPh$_3$-POL was selected as a representative sample to detect these functional sites. The pore structure and dispersion of Rh ions in Rh/*m*-3vPPh$_3$-POL were characterized through SEM, TEM and HADDF-STEM. The SEM images of Rh/*m*-3vPPh$_3$-POL and used Rh/*m*-3vPPh$_3$-POL (Fig. S2a and b†) reveal that the hierarchical porosity of *m*-3vPPh$_3$-POL is maintained well after immobilizing Rh ions and even after the reaction. The TEM images of Rh/*m*-3vPPh$_3$-POL and used Rh/*m*-3vPPh$_3$-POL (Fig. S2c and d†) display that Rh ions are highly dispersed in *m*-3vPPh$_3$-POL. The HADDF-STEM images and HADDF-EDS element maps of Rh/*m*-3vPPh$_3$-POL and used Rh/*m*-3vPPh$_3$-POL (Fig. S2e and f†) further confirm that P atoms are uniformly dispersed in the 3vPPh$_3$-POL framework, which provide abundant coordinating sites to coordinate with Rh ions and promote Rh ions to uniformly distributed as a single site. It is worth mentioning that the hierarchical porosity of *m*-3vPPh$_3$-POL is preserved after the reaction, demonstrating the superior structure stability of 3vPPh$_3$-POLs. Also, the abundant uncovered P atoms in 3vPPh$_3$-POLs are ready to coordinate with Rh ions and fix them as a single site; therefore, the microenvironment of the PPh$_3$ moiety in 3vPPh$_3$-POLs plays an important role in their properties and especially in their catalysis performance.

The ^{31}P MAS NMR spectrum of *m*-3vPPh$_3$-POL exhibits two signals (Fig. 4a), one is a strong signal at −3 ppm, which is attributed to P atoms in the *m*-3vPPh$_3$-POL framework, the other is a small peak at 25 ppm, which could be assigned to the slight oxidation of phosphorus (P═O).[26] A signal at 30 ppm is raised in Rh/*m*-3vPPh$_3$-POL, and increased after syngas treatment. In the used Rh/*m*-3vPPh$_3$-POL, the signal intensity at 30 ppm remains unchanged. By spectrum fitting, the peaks between 29 to 34 ppm are assigned to P multiply coordinated with Rh,[34,35] confirming that there are multiple coordination bonds between Rh and P in Rh/*m*-3vPPh$_3$-POL, which leads to the formation of Rh–P complexes and is beneficial for catalysis. Compared with *m*-3vPPh$_3$-POL, *p*-3vPPh$_3$-POL exhibits a little change in its ^{31}P MAS NMR spectra (Fig. 4b). The P in *p*-3vPPh$_3$-POL shows a peak at −6 ppm and a peak of P═O at 23 ppm. Moreover, a peak at 28 ppm appears in the fresh Rh/*p*-3vPPh$_3$-POL, it is shifted to 30 ppm and increased after syngas treatment, and then maintains its strength but is shifted back to 28 ppm after the reaction,[36] indicating that Rh is also multiply coordinated with P in *p*-3vPPh$_3$-POL, but the Rh–P complexes are different from those in *m*-3vPPh$_3$-POL. Though the ^{31}P MAS NMR spectrums confirm that Rh is multiply coordinated with P in both 3vPPh$_3$-POLs, P atoms in *p*-3vPPh$_3$-POL are more electronegative than those in

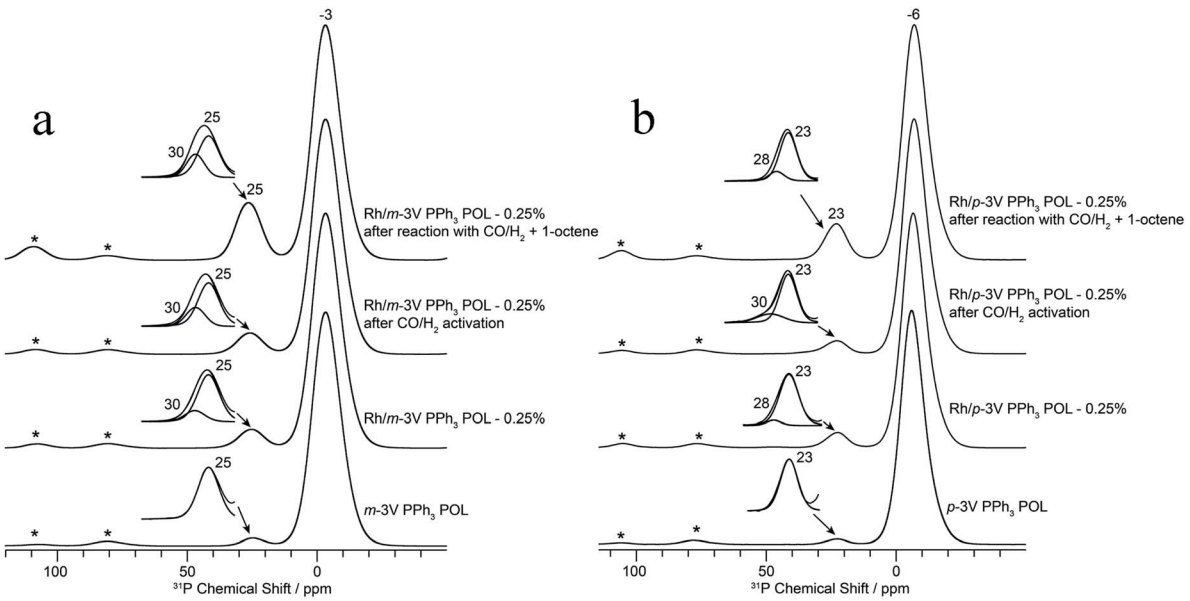

Fig. 4 (a) Changes in the ^{31}P MAS NMR spectra of *m*-3vPPh$_3$-POL and Rh/*m*-3vPPh$_3$-POL in different stages. (b) Changes in the ^{31}P MAS NMR spectra of *p*-3vPPh$_3$-POL and Rh/*p*-3vPPh$_3$-POL in different stages.

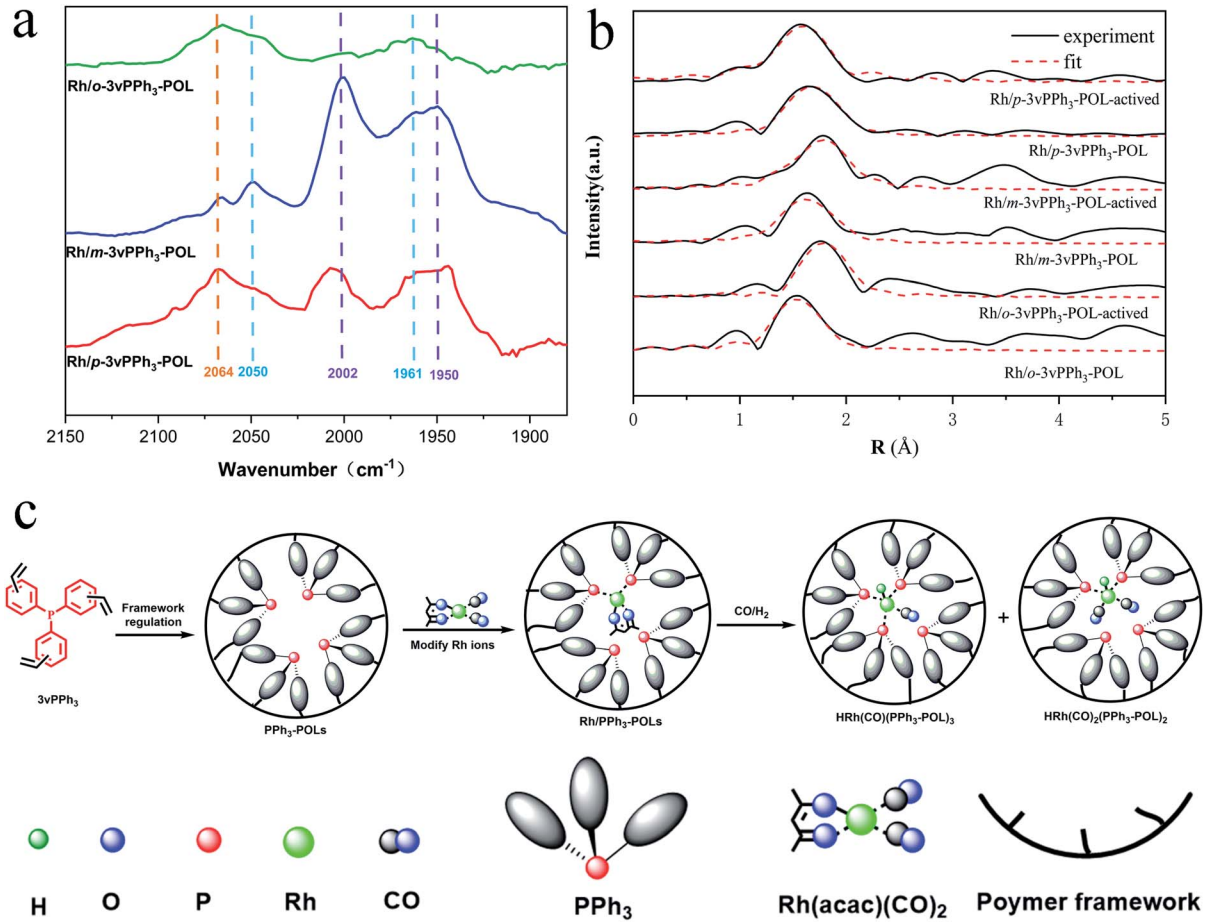

Fig. 5 (a) The *in situ* FT-IR spectra of Rh/3vPPh$_3$-POLs; the samples were purged with nitrogen at 383 K, and the background spectra were collected. Then, the samples were allowed to absorb syngas (CO/H$_2$ = 1 : 1) for 1 h and purged with nitrogen, and collected every 5 min until the spectrogram was unchanged. (b) The Rh K-edge k_3-weighted Fourier transform spectra of EXAFS; the activated samples were treated with syngas. (c) The preparation method, difference in coordination state and the Rh–P complexes among Rh/3vPPh$_3$-POLs.

m-3vPPh$_3$-POL. In a word, the microenvironment of the PPh$_3$ moiety is regulated by changing the position of the cross-linkers (vinyl groups) attached to the PPh$_3$ monomer, which influences the interaction between Rh ions and P atoms.

To discover the interaction between 3vPPh$_3$-POLs and Rh ions, we compared the change in P 2p binding energy of 3vPPh$_3$-POLs with the use of XPS (Fig. S3†). After modifying with 0.25 wt% Rh ions, the P 2p binding energy of all the three 3vPPh$_3$-POLs is increased by 0.1 eV, respectively, suggesting that there is interaction between 3vPPh$_3$-POLs and Rh ions, which is derived from the coordination between Rh ions and P atoms in 3vPPh$_3$-POLs.

As is known, Rh ions are capable of coordinating with P atoms and forming different kinds of Rh–P complexes, which may coexist in equilibrium in a homogeneous system.[37,38] To further disclose the differences in the Rh–P complexes among the three 3vPPh$_3$-POLs, characterization of the Rh–P complex was carried out by means of *in situ* FT-IR, as shown in Fig. 5a. The samples were *in situ* treated with syngas (CO : H$_2$ = 1 : 1) for 1 h in a cell at 383 K, then N$_2$ was introduced to replace syngas. The wavenumbers of the observed signals are indicated and assigned to the corresponding species and displayed in Table 2. There are four peaks that could be assigned to the HRh(CO)$_2$(PPh$_3$-POL)$_2$ species.[39] An equilibrium of two trigonal-bipyramidal isomers exists in the HRh(CO)$_2$(PPh$_3$-POL)$_2$ compound and each of the isomers has two peaks. The *ee*-HRh(CO)$_2$(PPh$_3$-POL)$_2$ species at 1961 cm^{-1} and 2050 cm^{-1} contains two equatorial phosphine ligands while the *ea*-HRh(CO)$_2$(PPh$_3$-POL)$_2$ species at 1950 cm^{-1} and 2002 cm^{-1} contains an equatorial and an apical phosphine ligand. The HRh(CO)(PPh$_3$-POL)$_3$ species has one characteristic peak at 2064 cm^{-1}. After the treatment with syngas, all of the Rh/3vPPh$_3$-POLs possess the *ea*-HRh(CO)$_2$(PPh$_3$-POL)$_2$ species, *ee*-HRh(CO)$_2$(PPh$_3$-POL)$_2$ species and HRh(CO)(PPh$_3$-POL)$_3$

Table 2 Assignments of the IR bands observed after syngas absorption processes over Rh/PPh$_3$-POLs

Rh–P species	Wave numbers (cm^{-1})	Ref.
ee-HRh(CO)$_2$(PPh$_3$POL)$_2$	1961, 2050	37 and 43
ea-HRh(CO)$_2$(PPh$_3$POL)$_2$	1950, 2002	37 and 43
HRh(CO)(PPh3POL)$_3$	2064	44

Table 3 The curve-fitting analysis of the EXAFS traces

Sample	Coordination	CN	R (Å)	σ^2 ($\times 10^{-3}$ Å^2)	R-Factor (%)
Rh/*p*-3vPPh$_3$-POL	Rh–P	2.6	2.34	6.6	0.65
	Rh–O	1.9	2.08	3.5	
Rh/*p*-3vPPh$_3$-POL-actived	Rh–P	2.7	2.24	4.0	1.81
	Rh–C	1.3	1.72	9.0	
Rh/*m*-3vPPh$_3$-POL	Rh–P	2.4	2.34	5.9	0.77
	Rh–O	2.0	2.08	4.2	
Rh/*m*-3vPPh$_3$-POL-actived	Rh–P	2.2	2.31	3.8	1.73
	Rh–C	1.9	1.72	3.1	
Rh/*o*-3vPPh$_3$-POL	Rh–P	2.9	2.33	6.7	0.83
	Rh–O	1.7	2.08	4.5	
Rh/*o*-3vPPh$_3$-POL-actived	Rh–P	2.8	2.31	3.8	1.45
	Rh–C	1.3	1.77	1.3	

species. However, compared with *p*-3vPPh$_3$-POL and *o*-3vPPh$_3$-POL, *m*-3vPPh$_3$-POL presents an apparent tendency to form the HRh(CO)$_2$(PPh$_3$-POL)$_2$ species rather than the HRh(CO)(PPh$_3$-POL)$_3$ species, which means that Rh in *m*-3vPPh$_3$-POL has a stronger affinity with CO.[40–42] The *in situ* FT-IR spectra of the three Rh/3vPPh$_3$-POLs show great difference, illustrating that the microenvironment of the PPh$_3$ moiety in the three 3vPPh$_3$-POLs is diverse, which endows Rh/3vPPh$_3$-POLs with different ratios of Rh–P complexes and consequently distinctive catalytic performance.

To get a more specific understanding about the coordination state of Rh with P species in 3vPPh$_3$-POLs, EXAFS characterization was employed. As shown in Fig. 5b, no Rh–Rh bonds can be detected in any of the tested samples, indicating that Rh ions are dispersed exclusively as a single site by P species in 3vPPh$_3$-POLs. According to the fitting result (Table 3), in the fresh Rh/3vPPh$_3$-POL catalysts, Rh atom is coordinated with O atoms and P atoms, in which the Rh–P bonds are derived from Rh coordinated with P species in 3vPPh$_3$-POLs and Rh–O bonds are derived from acetylacetone (acac) of Rh(acac)(CO)$_2$.[26] After syngas treatment, the coordination state of Rh atoms changes a lot. In the Rh/*p*-3vPPh$_3$-POL-actived sample, each Rh atom is coordinated with 1.3 C atoms and 2.7 P atoms, while in the Rh/*o*-3vPPh$_3$-POL-actived sample, each Rh atom is coordinated with 1.3 C atom and 2.8 P atoms. Nevertheless, each Rh atom is coordinated with 1.9 C atoms and 2.2 P atoms in the Rh/*m*-3vPPh$_3$-POL-actived sample, which is significantly different from those in the Rh/*p*-3vPPh$_3$-POL-actived and Rh/*o*-3vPPh$_3$-POL-actived samples. The proportion of HRh(CO)$_2$(PPh$_3$-POL)$_2$ and HRh(CO)(PPh$_3$-POL)$_3$ species in different Rh/3vPPh$_3$-POLs are fitted and listed in Table 4, which illustrates that each of the Rh/3vPPh$_3$-POLs possesses a different composition of Rh–P complexes. It is more likely to generate the HRh(CO)$_2$(PPh$_3$-POL)$_2$ species rather than the HRh(CO)(PPh$_3$-POL)$_3$ species on Rh/*m*-3vPPh$_3$-POL-actived, while relatively more HRh(CO)(PPh$_3$-POL)$_3$ species are generated on Rh/*p*-3vPPh$_3$-POL-actived and Rh/*o*-3vPPh$_3$-POL-actived. The difference in coordination state and the Rh–P complexes among Rh/3vPPh$_3$-POLs are illustrated in Fig. 5c.

The results of MAS NMR, *in situ* FTIR and EXAFS spectra prove that the microenvironments of the PPh$_3$ moiety in the three 3vPPh$_3$-POLs are various, which is influenced by the position of the cross-linkers attached to the PPh$_3$ monomer, and the subsequent Rh/3vPPh$_3$-POL catalysts may display dissimilar behaviors in catalytic reactions. Thus, the strategy of regulating the structure and property of POPs by simply changing the position of the cross-linkers attached to the monomer has been successfully established.

3.3 Performance tests of 3vPPh$_3$-POLs in hydroformylation

It is commonly recognized that the hydroformylation reaction is sensitive to the Rh–P complexes; as a consequence, the hydroformylation reaction was selected as a probe reaction to assess the difference in 3vPPh$_3$-POLs in catalytic performance.

Initially, Rh(CO)$_2$(acac) was employed in the hydroformylation of 1-octene in a homogeneous system, shown in Fig. 6a (detailed data are listed in Table S1†). The conversion of 1-octene is 99% while the aldehyde selectivity is only 8.5%, and the *l*/*b* ratio is 0.6; therefore, 1-octene is mainly converted to isoalkenes and alkane by Rh(CO)$_2$(acac). Then, Rh(CO)$_2$(acac) was coordinated with the three 3vPPh$_3$ monomers in the

Table 4 The proportion of HRh(CO)$_2$(PPh$_3$-POL)$_2$ and HRh(CO)(PPh$_3$-POL)$_3$ species in different activated Rh/3vPPh$_3$-POLs

	Active species proportion (%)	
Samples	HRh(CO)$_2$(PPh$_3$-POL)$_2$	HRh(CO)(PPh$_3$-POL)$_3$
Rh/*p*-3vPPh$_3$-POL-actived	30	70
Rh/*m*-3vPPh$_3$-POL-actived	85	15
Rh/*o*-3vPPh$_3$-POL-actived	25	75

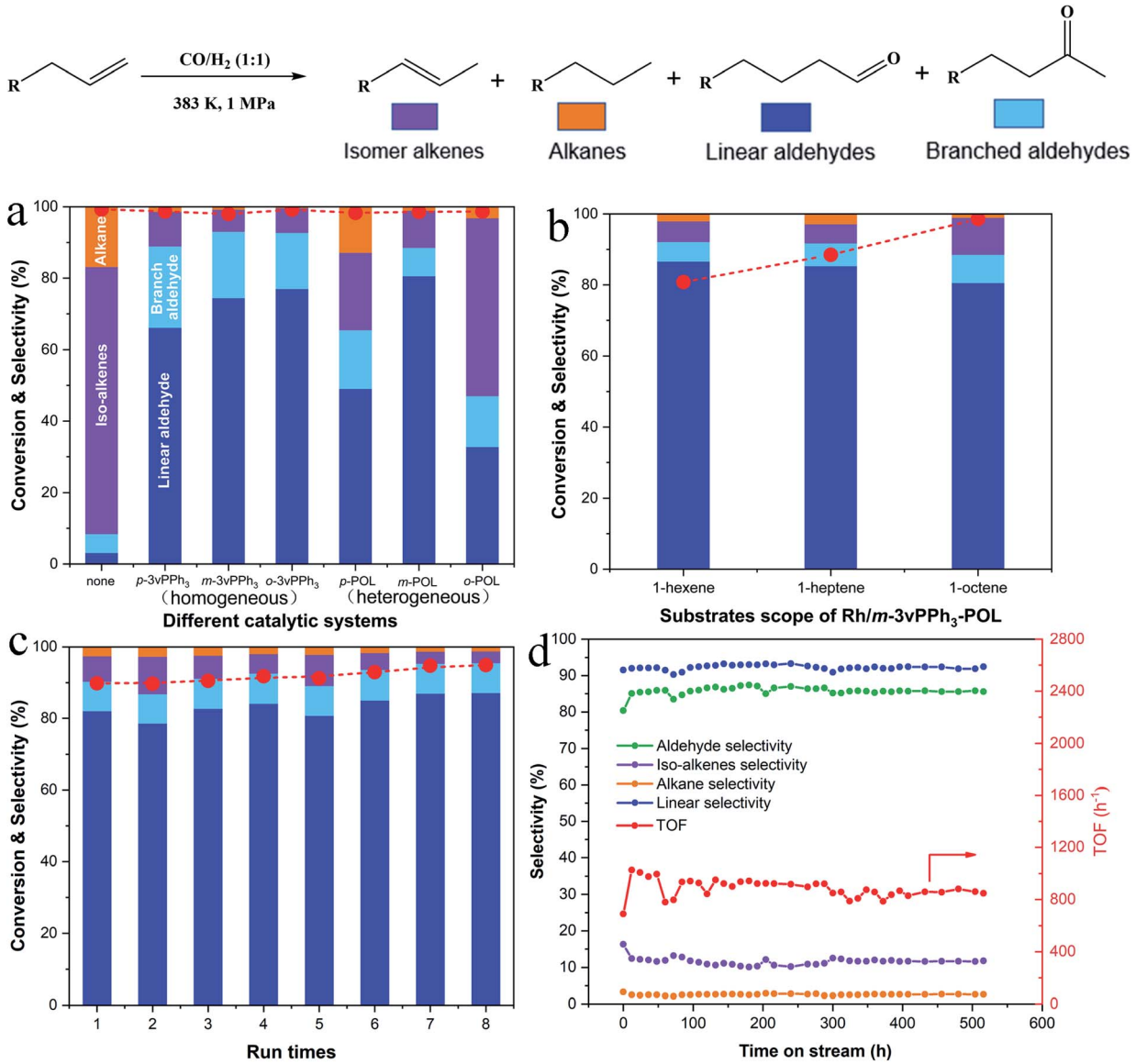

Fig. 6 (a) Test of different Rh catalysts in hydroformylation of 1-octene. None is Rh ions; *p*-3vPPh$_3$ is Rh-*p*-3vPPh$_3$; *m*-3vPPh$_3$ is Rh-*m*-3vPPh$_3$; *o*-3vPPh$_3$ is Rh-*o*-3vPPh$_3$; *p*-POL is Rh/*p*-3vPPh$_3$-POL; *m*-POL is Rh/*m*-3vPPh3-POL; *o*-POL is *o*-3vPPh3-POL. (b) Rh/*m*-3vPPh$_3$-POL catalytic performance test in long-chain olefin hydroformylation reactions. (c) Rh/*m*-3vPPh$_3$-POL recycle performance in 1-octene hydroformylation. Reaction conditions: substrate (1.0 g), toluene (5.0 g), Rh catalysts (0.060 g, Rh wt% = 0.25%), T = 383 K, P = 1.0 MPa, t = 12 h. Conversion is indicated by the circles, selectivity is indicated by the bars. (d) Stability tests of Rh/*m*-3vPPh$_3$-POL in 1-octene hydroformylation reaction in a fixed-bed reactor. Reaction conditions: substrate (0.8 mL h^{-1}), syngas (1000.0 mL h^{-1}), catalyst (0.30 g, Rh wt% = 0.25%), T = 383 K, P = 1.0 MPa. The products were collected in a cooling tank and analysed every 12 h.

hydroformylation of 1-octene in a homogeneous system. With the introduction of *p*-3vPPh$_3$, the aldehyde selectivity and *l*/*b* ratio are increased to 89.0% and 2.9 on Rh-*p*-3vPPh$_3$, respectively. Comparatively, Rh-*m*-3vPPh$_3$ displays a higher aldehyde selectivity (93.1%) and *l*/*b* ratio (4.0). Also, an aldehyde selectivity of 92.8% and an *l*/*b* ratio of 4.9 are obtained by using Rh-*o*-3vPPh$_3$.

After that, 3vPPh$_3$-POLs were engaged to support and coordinate with Rh(CO)$_2$(acac), named Rh/3vPPh$_3$-POLs, and applied in the heterogeneous hydroformylation of 1-octene. Compared with the corresponding homogeneous Rh-3vPPh$_3$ catalysts, Rh/3vPPh$_3$-POLs show considerably different catalytic performance in the heterogeneous system. Rh/*p*-3vPPh$_3$-POL displays an aldehyde selectivity of 65.5% and an *l*/*b* ratio of 3.0. However, only 47.1% aldehyde selectivity and an *l*/*b* ratio of 2.3 are attained by Rh/*o*-3vPPh$_3$-POL, which may be caused by its lower BET surface area and poor porosity. To our delight, the highest aldehyde selectivity (88.6%) and *l*/*b* ratio (*ca.* 10) are obtained on the Rh/*m*-3vPPh$_3$-POL catalyst. Obviously, the excellent performance of Rh/*m*-3vPPh$_3$-POL could be assigned to its unique structure and microenvironment of the PPh$_3$ moiety in *m*-3vPPh$_3$-POL.

Next, Rh/*m*-3vPPh$_3$-POL was employed to optimize the reaction conditions. As shown in Table S2,† with the syngas

Table 5 Rh concentration in fresh and used catalysts

Sample	Rh concentration (%)
Rh/*m*-3vPPh$_3$-POL (fresh sample)	0.2656
Rh/*m*-3vPPh$_3$-POL (used sample)	0.2615

pressure increasing, aldehyde selectivity is improved while *l*/*b* ratio is repressed. Table S3† exhibits that enhanced temperature could increase the conversion of 1-octene, but decrease the aldehyde selectivity. The optimized syngas pressure was fixed at 1.0 MPa while the reaction temperature was fixed at 383 K. Under optimal conditions, the turnover frequency (TOF) is as high as 2221.6 h^{-1} (Table S4†), representing the superior activity of Rh/*m*-3vPPh$_3$-POL.

To extend the scope of Rh/*m*-3vPPh$_3$-POLs in the hydroformylation reaction, we also employed 1-hexene, 1-heptene and 1-octene as substrates in an autoclave reactor, and the result is shown in Fig. 6b. For the hydroformylation of 1-hexene, 1-heptene and 1-octene, the Rh/*m*-3vPPh$_3$-POL catalysts display high selectivity of aldehydes (above 88.6%), high *l*/*b* ratio (above 10) and low selectivity of alkanes (lesser than 2.8%). The main by-products are isomeric alkenes, which can be converted to the corresponding initial substrates.

Recyclability is an important index for catalysts. As shown in Fig. 6c, in recycling tests, Rh/*m*-3vPPh$_3$-POL can be reused at least 8 times with high selectivity, activity and *l*/*b* ratio. The used Rh/*m*-3vPPh$_3$-POL was analyzed by ICP-OES, which showed that the Rh ions are durably fixed by *m*-3vPPh$_3$-POL (Table 5), probably owing to the high density of P atoms and the multiple Rh–P coordination bonds.

To exploit the stability and feasibility of Rh/*m*-3vPPh$_3$-POL for industrial applications, we also performed the hydroformylation of 1-octene in a fixed-bed reactor. The simple flowchart is shown in Scheme S1,† and the reaction temperature and pressure were fixed at 383 K and 1.0 MPa, respectively, the LHSV of 1-octene was fixed at 0.4 h^{-1}, and the GHSV of syngas ($CO : H_2 = 1 : 1$) was fixed at 500 h^{-1}. As shown in Fig. 6d, the selectivity of aldehydes and linear selectivity (the proportion of linear aldehyde in all aldehydes) are more than 85% and 90%, respectively, during the time-on-stream over 500 h. During the stability test, the selectivity of isomerized alkenes is about 10% to 12%, and the alkane selectivity is below 3%. The TOF of aldehyde on Rh/*m*-3vPPh$_3$-POL is above 800 h^{-1} during the test. The fixed-bed reactor test further demonstrated the excellent stability of Rh/*m*-3vPPh$_3$-POL, implying its great potential for industrial application.

4 Conclusions

In this work, we provide a new strategy to regulate the structure and properties of POPs by changing the position of the cross-linkers (vinyl groups) attached to the corresponding monomer. According to our strategy, we obtained three vinyl functional 3vPPh$_3$ monomers, then fabricated three 3vPPh$_3$-POLs samples through polymerization. The resulting rigid 3vPPh$_3$-POLs possessed different BET surface areas, pore volumes and pore structures. Moreover, the microenvironment of the PPh$_3$ moiety, the negativity and the hindrance of P in the three 3vPPh$_3$-POLs were different, which led to their different abilities to coordinate with Rh to catalyze some hydroformylation reactions. Remarkable improvement in chemo-selectivity and regioselectivity in the hydroformylation reaction were achieved on Rh/*m*-3vPPh$_3$-POL, and over 500 h performance tests further confirmed their prominent stability and industrial application potential. Given the efficiency and feasibility of this regulation strategy, we expect that the strategy of regulating the position of cross-linkers will be instructive in designing functional POP materials.

Conflicts of interest

There are no conflicts to declare.

Acknowledgements

This work was supported by the National Natural Science Foundation of China (no. 91845101, 22002152), the Transformational Technologies for Clean Energy and Demonstration", Strategic Priority Research Program of the Chinese Academy of Sciences, grant no. XDA 21020900, the Strategic Priority Research Program of the Chinese Academy of Sciences, grant no. XDB 17000000, and DICP & QIBEBT (grant no. DICP & QIBEBT UN201704). +shanghai. Rh K-edge X-ray absorption fine structure (EXAFS and XANES) spectra were obtained at the BL14W1 beamline of Shanghai Synchrotron Radiation Facility (SSRF), Shanghai Institute of Applied Physics (SINAP), Chinese Academy of Sciences. Technical support and helpful discussion by Prof. Zheng Jiang are gratefully acknowledged.

Notes and references

1 R. Luo, M. Chen, X. Liu, W. Xu, J. Li, B. Liu and Y. Fang, *J. Mater. Chem. A*, 2020, **8**, 18408–18424.
2 Z. F. Sha, S. Q. Qiu, Q. Zhang, Z. Y. Huang, X. Cui, Y. K. Yang and Z. Q. Lin, *J. Mater. Chem. A*, 2019, **7**, 23019–23027.
3 L. P. Tang, S. Yang, D. Liu, C. Wang, Y. Q. Ge, L. M. Tang, R. L. Zhou and H. Zhang, *J. Mater. Chem. A*, 2020, **8**, 14356–14383.
4 R. Dawson, T. Ratvijitvech, M. Corker, A. Laybourn, Y. Z. Khimyak, A. I. Cooper and D. J. Adams, *Polym. Chem.*, 2012, **3**, 2034–2038.
5 Z. Chang, D. S. Zhang, Q. Chen and X. H. Bu, *Phys. Chem. Chem. Phys.*, 2013, **15**, 5430–5442.
6 X. Q. Zou, H. Ren and G. S. Zhu, *Chem. Commun.*, 2013, **49**, 3925–3936.
7 R. Tao, X. Ma, X. Wei, Y. Jin, L. Qiu and W. Zhang, *J. Mater. Chem. A*, 2020, **8**, 17360–17391.
8 J. W. Bai, W. P. Zhang, X. F. Ma, L. Q. Chen, L. J. Liu and C. H. Zhang, *Microporous Mesoporous Mater.*, 2020, **294**, 7.
9 H. Ye, C. Zhang, C. Huo, B. Zhao, Y. Zhou, Y. Wu and S. Shi, *Polym. Rev.*, 2020, DOI: 10.1080/15583724.2020.1821059.

10 S. H. Luo, Z. T. Zeng, G. M. Zeng, Z. F. Liu, R. Xiao, P. Xu, H. Wang, D. L. Huang, Y. Liu, B. B. Shao, Q. H. Liang, D. B. Wang, Q. Y. He, L. Qin and Y. K. Fu, *J. Mater. Chem. A*, 2020, **8**, 6434–6470.
11 K. Geng, T. He, R. Liu, S. Dalapati, K. T. Tan, Z. Li, S. Tao, Y. Gong, Q. Jiang and D. Jiang, *Chem. Rev.*, 2020, **120**, 8814–8933.
12 A. P. Cote, A. I. Benin, N. W. Ockwig, M. O'Keeffe, A. J. Matzger and O. M. Yaghi, *Science*, 2005, **310**, 1166–1170.
13 S. Wan, J. Guo, J. Kim, H. Ihee and D. L. Jiang, *Angew. Chem., Int. Ed.*, 2009, **48**, 5439–5442.
14 A. F. M. El-Mahdy, M. B. Zakaria, H.-X. Wang, T. Chen, Y. Yamauchi and S.-W. Kuo, *J. Mater. Chem. A*, 2020, **8**, 25148–25155.
15 P. Kuhn, M. Antonietti and A. Thomas, *Angew. Chem., Int. Ed.*, 2008, **47**, 3450–3453.
16 S. Das, P. Heasman, T. Ben and S. L. Qiu, *Chem. Rev.*, 2017, **117**, 1515–1563.
17 D. Zhang, L. Tao, J. Ju, Y. Wang, Q. Wang and T. Wang, *Polymer*, 2015, **60**, 234–240.
18 C. D. Wood, B. Tan, A. Trewin, F. Su, M. J. Rosseinsky, D. Bradshaw, Y. Sun, L. Zhou and A. I. Cooper, *Adv. Mater.*, 2008, **20**, 1916–1921.
19 P. M. Budd, E. S. Elabas, B. S. Ghanem, S. Makhseed, N. B. McKeown, K. J. Msayib, C. E. Tattershall and D. Wang, *Adv. Mater.*, 2004, **16**, 456–459.
20 B. S. Ghanem, N. B. McKeown, P. M. Budd, N. M. Al-Harbi, D. Fritsch, K. Heinrich, L. Starannikova, A. Tokarev and Y. Yampolskii, *Macromolecules*, 2009, **42**, 7881–7888.
21 J. Chen, T. Qiu, W. Yan and C. F. J. Faul, *J. Mater. Chem. A*, 2020, **8**, 22657–22665.
22 Y. B. Zhou, Y. Q. Wang, L. C. Ning, Z. C. Ding, W. L. Wang, C. K. Ding, R. H. Li, J. J. Chen, X. Lu, Y. J. Ding and Z. P. Zhan, *J. Am. Chem. Soc.*, 2017, **139**, 3966–3969.
23 M. Jiang, L. Yan, Y. J. Ding, Q. Sun, J. Liu, H. J. Zhu, R. H. Lin, F. S. Xiao, Z. Jiang and J. Y. Liu, *J. Mol. Catal. A: Chem.*, 2015, **404**, 211–217.
24 Y. Q. Wang, L. Yan, C. Y. Li, M. Jiang, Z. Zhao, G. J. Hou and Y. J. Ding, *J. Catal.*, 2018, **368**, 197–206.
25 C. Y. Li, K. J. Sun, W. L. Wang, L. Yan, X. P. Sun, Y. Q. Wang, K. Xiong, Z. P. Zhan, Z. Jiang and Y. J. Ding, *J. Catal.*, 2017, **353**, 123–132.
26 C. Y. Li, L. Yan, L. L. Lu, K. Xiong, W. L. Wang, M. Jiang, J. Liu, X. G. Song, Z. P. Zhan, Z. Jiang and Y. J. Ding, *Green Chem.*, 2016, **18**, 2995–3005.
27 Z. Ren, Y. Lyu, X. E. Song, Y. Liu, Z. Jiang, R. H. Lin and Y. J. Ding, *Adv. Mater.*, 2019, **31**, 6.
28 C. Y. Li, K. Xiong, L. Yan, M. Jiang, X. G. Song, T. Wang, X. K. Chen, Z. P. Zhan and Y. J. Ding, *Catal. Sci. Technol.*, 2016, **6**, 2143–2149.
29 M. Jiang, Y. J. Ding, L. Yan, X. G. Song and R. H. Lin, *Chin. J. Catal.*, 2014, **35**, 1456–1464.
30 M. Jiang, L. Yan, X. P. Sun, R. H. Lin, X. G. Song, Z. Jiang and Y. J. Ding, *React. Kinet., Mech. Catal.*, 2015, **116**, 223–234.
31 Q. Sun, Z. F. Dai, X. J. Meng and F. S. Xiao, *Catal. Today*, 2017, **298**, 40–45.
32 S. V. Dvinskikh, H. Zimmermann, A. Maliniak and D. Sandstrom, *J. Magn. Reson.*, 2004, **168**, 194–201.
33 Y. Q. Wang, L. Yan, C. Y. Li, M. Jiang, W. L. Wang and Y. J. Ding, *Appl. Catal., A*, 2018, **551**, 98–105.
34 G. Wu and R. E. Wasylishen, *Inorg. Chem.*, 1992, **31**, 145–148.
35 G. Wu and R. E. Wasylishen, *Organometallics*, 1992, **11**, 3242–3248.
36 Y. S. Varshavsky, T. G. Cherkasova, N. A. Buzina and L. S. Bresler, *J. Organomet. Chem.*, 1994, **464**, 239–245.
37 C. K. Brown and G. Wilkinson, *J. Chem. Soc. A*, 1970, 2753–2764.
38 J. M. Brown and A. G. Kent, *J. Chem. Soc., Perkin Trans. 2*, 1987, 1597–1607, DOI: 10.1039/p29870001597.
39 E. B. Walczuk, P. C. J. Kamer and P. van Leeuwen, *Angew. Chem., Int. Ed.*, 2003, **42**, 4665–4669.
40 L. A. Gerritsen, A. Vanmeerkerk, M. H. Vreugdenhil and J. J. F. Scholten, *J. Mol. Catal.*, 1980, **9**, 139–155.
41 L. A. van der Veen, M. D. K. Boele, F. R. Bregman, P. C. J. Kamer, P. van Leeuwen, K. Goubitz, J. Fraanje, H. Schenk and C. Bo, *J. Am. Chem. Soc.*, 1998, **120**, 11616–11626.
42 J. M. Brown and A. G. Kent, *J. Chem. Soc., Perkin Trans. 2*, 1987, 1597–1607, DOI: 10.1039/p29870001597.
43 L. Yan, Y. J. Ding, L. W. Lin, H. J. Zhu, H. M. Yin, X. M. Li and Y. Lu, *J. Mol. Catal. A: Chem.*, 2009, **300**, 116–120.
44 E. B. Walczuk, P. C. J. Kamer and P. van Leeuwen, *Angew. Chem., Int. Ed.*, 2003, **42**, 4665–4669.

